Biosensors & Bioelectronics **10** (1995) 903–916

Spectroscopic and surface-analytical characterization of self-assembled layers on Au

Silvia Mittler-Neher, Jürgen Spinke#, Martha Liley§, Gabriele Nelles, Michael Weisser, Roberta Back, Gerhard Wenz† & Wolfgang Knoll*

Max-Planck-Institute für Polymerforschung, Ackermann Weg 10, 55128 Mainz, Germany.
Tel: 61 31 379 164 Fax: 61 31 379 100.

Abstract: Future devices for electronic, photonic or other "intelligent" application involving (bio-) organic materials require nano-fabrication, -manipulation, -patterning and -functionalization techniques. Supramolecular assemblies, aggregates, small molecules and ions have to be controlled with regard to their structure, order and dynamic behaviour down to the molecular or even atomic level.

This contribution summarizes some of our activities aiming at a better understanding of the physical and chemical properties of functionalized and patterned surfaces. We focus on structure/order–property/function relations in such complex systems as interfaces and thin film architectures. Optical techniques (surface plasmon–spectroscopy) as well as surface analytical techniques (cyclic voltammetry and contact angle investigations) are introduced and demonstrated as powerful tools for the characterization of these interfaces and thin films.

Examples will be given covering self-assembly monolayers and molecular recognition—as well as complexation—reactions.

Keywords: evanescent wave techniques, self-assembled monolayers, guest–host-interaction

INTRODUCTION

The growing interest in ultrathin organic films for various fields of modern technology, e.g. for integrated optics and biotechnology, requires highly sensitive characterization techniques. The investigation of monomolecular films, highly sophisticated microarchitectures and structures is an actual field of research [1]. For possible application of these nanomaterials in biophysics and microtechnology a careful control of the molecular structure and the microscopic order of the ultrathin films is required. To meet these ends many different experimental techniques have been developed in recent years to gain sensitivity in the monolayer range. Optical tech-

Present addresses: #Roche Diagnostics Systems, Hoffman La Roche, 4002 Basel, Switzerland.
§ Ecole Polytechnique Federal Lausanne, Department de Chemie, EPFL-Ecublens, 1015 Lausanne, Switzerland.
†Polymer Institute der Universität Karlsruhe, Hertzstr. 16, 76187 Karlsruhe, Germany.
*The Institute of Physical and Chemical Research (RIKEN), Wako, Saitama 351-01, Japan.

0956–5663/95/$09.50

niques using the evanescent fields of surface plasmons and waveguide modes [2,3] as well as the nano-scanning techniques like scanning tunneling microscopy (STM) [4], scanning atomic force microscopy (AFM) [5] and scanning near field optical microscopy (SNOM) [6] have been proven to be particularly well suited for ultrathin film investigations.

This paper focuses on optical evanescent wave spectroscopy, especially on surface plasmon spectroscopy. Chemical surface sensitive methods like cyclic voltammetry [7] and contact angle measurements [8] are used in addition to gain further information. The examples concern the build up of well-ordered, highly organized mono- and multi-layer assemblies prepared by self-assembly and/or complexation processes [9,10]. Reversible and nonreversible interfacial binding and molecular recognition reactions are followed kinetically [11,12].

This article first introduces the physics of evanescent light in general, and of surface plasmons and waveguide modes in particular. It is demonstrated with two major examples that the excitation of surface plasmons and the data evaluated from there together with surface chemical methods provide valuable information about the architecture of an interface.

EVANESCENT WAVES: SURFACE PLASMONS AND WAVEGUIDE MODES

The simplest case for the existence of an evanescent wave is the well-known total internal reflection of a plane electromagnetic wave at the base of a glass prism (index of refraction n_1) in contact with an optically less dense medium (with $n_2 < n_1$). This geometry is schematically sketched in Fig. 1a (top). If the reflected light intensity is recorded as a function of the angle of incidence, θ, the reflectivity, R, reaches unity as one approaches the critical angle, θ_c, for total reflection (Fig. 1a, bottom). A closer inspection of the distribution of the electric field, E, in the close vicinity of the interface shows that above θ_c the electrical field, and therefore the intensity of the light does not fall abruptly to zero, but there is instead a harmonic wave travelling parallel to the surface with an amplitude decaying exponentially normal to the surface. The penetration depth, l, defined by the 1/e attenuation, is given by

$$l = \frac{\lambda}{2\pi\sqrt{(n_1 \sin\theta)^2 - 1}} \quad (1)$$

and found to be in the order of the wavelength of light. This type of wave is called an evanescent wave [13].

One way of introducing surface plasmons (plasmon surface polaritons [14] or PSPs), especially in the experimental setup called the Kretschmann configuration [15] (see Fig. 1b top) is to note that the nearly free electron gas in a thin (≈50 nm) metal film evaporated onto the base of a prism acts as an oscillator that can be driven by the electromagnetic wave impinging upon that interface. Therefore, we are dealing with a resonant excitation of a coupled state between the plasma oscillations and the photons: the plasmon surface polariton. This resonance phenomenon can clearly be seen in the ATR scan (attenuated total reflection, see bottom of Fig. 1b). Below θ_c the reflectivity is high because the metal film acts as a mirror with only little transmission. Above θ_c for total internal reflection a relatively narrow dip in the reflectivity curve at θ_0 indicates the resonant excitation of such a PSP wave at the metal–dielectricum interface. The coupling angle is given by the energy and momentum matching conditions between photons and surface plasmons:

$$k_{sp}^0 = k_{ph}^0 = n_1 \frac{\omega}{c} \sin\phi_0 \quad (2)$$

with k_{ph}^0 being the parallel component of the photon wave vector, $\hbar\omega$ the photon energy, c the speed of light and ϕ_0 the internal coupling angle (see Fig. 1b top).

Again, we are dealing with an evanescent wave propagating along the interface with a penetration depth into the dielectricum of the order of the wavelength. The resonance character of this excitation gives rise to an enhancement of the electric field at the interface by more than a factor of 10, which is the origin of the remarkable sensitivity enhancements obtainable, e.g. in Raman spectroscopy when working with PSP light [16,17]. Dissipative and radiative losses that these modes experience are also important. This leads to strong damping along the propagation direction [18,19].

Since we are dealing with well-defined modes obeying a known dispersion relation, ω versus k_{sp} [2,14], each photon of an energy $\hbar\omega_L$ allows for the resonant excitation of only one PSP

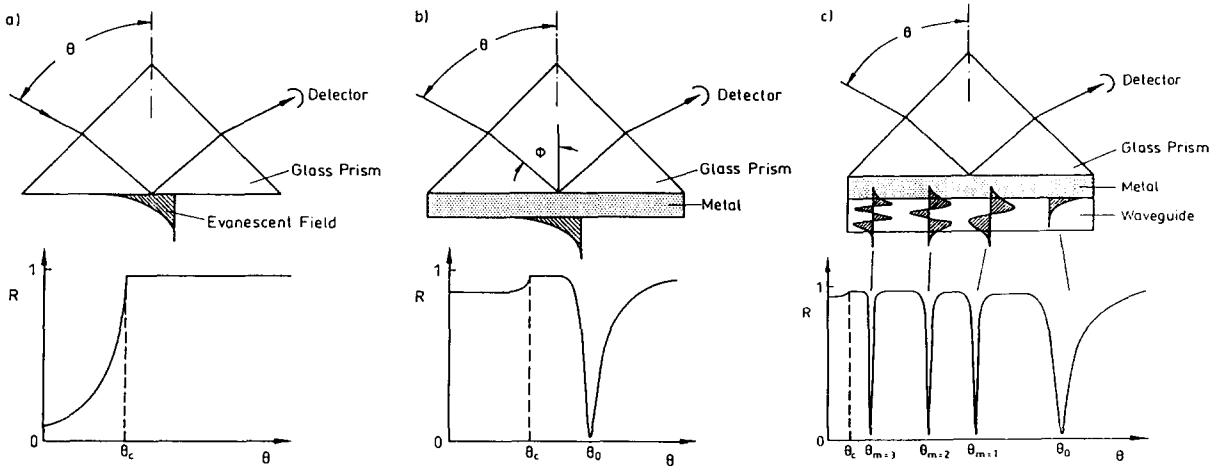

Fig. 1. Various configurations for evanescent wave optics: (a) (top) Total internal reflection of a plane wave at the base of a glass prism; (bottom) the reflectivity, R, recorded as a function of the angle of incidence shows the increase to unity at θ_c, the critical angle for total reflection. (b) ATR setup for the excitation of surface plasmons (PSPs) in Kretschmann geometry: (top) a thin metal film (thickness ≈50 nm) is evaporated onto the base of a glass prism and acts as a resonator driven by the photon field; (bottom) the resonant excitation of the PSP wave is seen in the reflectivity curve as a sharp dip at coupling angle θ_0. (c) (top) In addition to the PSP wave, various waveguide modes can be excited by this configuration as long as the dielectric layer is thick enough; (bottom) excitation of these modes can also be seen in the reflectivity curve as very sharp dips. Modes are indexed according to their number of nodes of their field distribution. Surface plasmons can only be excited with p-polarized light, whereas waveguide modes exist for s- and p-polarized light.

mode. This is schematically depicted in Fig. 2. The solid curve represents the dispersion relation of the surface plasmon at a metal (here gold)/air interface (PSP^0). The horizontal line at ω_L intersects the dispersion curve at k_{sp}^0 and thus defines the coupling angle θ_0. A thin dielectric layer causes a shift of the dispersion curve (PSP^1) to higher momentum

$$k_{sp}^1 = k_{sp}^0 + \Delta k_{sp} \quad (3)$$

which, according to equation 2, shifts the resonance to a higher angle θ_1. From this shift and a fit to Fresnel's equations, one can calculate the optical thickness (nd) of the layer [20]. Accurate conversion of this optical thickness requires knowledge of the refractive index of the film, a parameter which depends both on the material of the film and how closely packed it is. Therefore the results of adsorption experiments are average thicknesses. That does not necessarily imply that we believe that the film thickness varies. In the case of a closely packed monolayer of a molecule of well-known size, it is clear that the film thickness corresponds to the size of this molecule, while the actual parameter being varied is the density of that molecule within the layer. The greater the measured thickness of that layer, the more closely the film approaches the closed packed system we require and which we use to set our refractive index.

In Fig. 3 the scheme of the actual experimental setup is demonstrated for *in situ* surface plasmon characterization. Adsorption processes occuring at the gold surface can be followed in real time, by selecting an appropriate angle of incidence, θ_b, and monitoring the reflected intensity as a function of time. Knowledge of the form of the resonance curve allows this intensity to be interpreted as a shift in the angle of resonance.

If the thickness of the layer on the gold is increased, a new type of nonradiative modes, guided optical waves, can be observed. Figure 1c shows the electrical field distribution of a few modes in the top part. Generally, these modes can be excited if the light travelling inside such a thin slab configuration is totally reflected at both boundaries to the surrounding media and fulfills the well-known mode equation [21,22]:

$$kd + \beta_0 + \beta_1 = m\pi \quad (4)$$

with k being the wavevector of the mode of order m, d the thickness of the waveguide layer

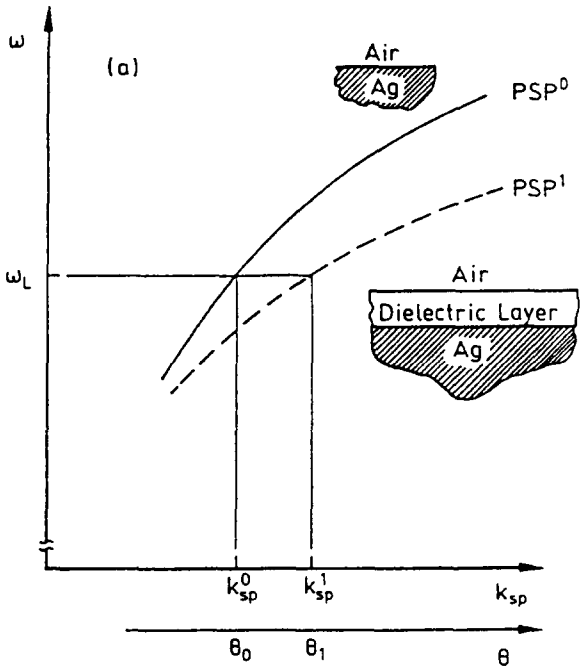

Fig. 2. Dispersion relation, ω versus k_{sp}, of PSPs at an Ag/air-(PSP^0, solid line) and at an Ag/dielectric layer/air-interface (PSP^1, broken line). Laser light of an energy $\hbar\omega_L$ couples at an angle θ_0 and θ_1, respectively, given by the energy and momentum matching condition (horizontal line at ω_L).

and $2\beta_i = r_i''/r_i'$ with $r_i = r_i' + ir_i''$ the complex reflection coefficients at the interfaces. The resonant excitation of these modes of different order m can be seen in the reflected intensity scan: narrow dips above θ_c indicate the existence of various guided waves.

Actually, optical waveguide modes are not evanescent, except for their two exponentially decaying tails reaching into both surrounding media. Because these modes are nonradiative they, too, need a dispersive element, a prism or a grating, to be coupled into the system. What makes optical waveguide modes a valuable diagnostic tool is that they can be excited with p- and s-polarized light, resulting in TM and TE modes, respectively. This means that for dielectric materials different components of the dielectric tensor within the waveguide structure can be probed. When there is no metal layer it is also possible to couple light into waveguide modes which propagate for centimetres [23]. This long propagation length can be used in integrated optical devices, even without the field enhancement through the metal, to integrate over changes on top or within the waveguide device [24,25,26].

CONTACT ANGLE MEASUREMENTS

Advancing and receding contact angles of water can be measured using a contact angle microscope under ambient conditions, while the volume of the drop is increased or decreased at a rate just large enough to result in a movement of the water/air/solid triple line. The contact angles mirror the hydrophilicity or hydrophobicity of the surface under investigation. Small angles indicate a hydrophilic surface, whereas high angles indicate a hydrophobic sample surface.

CYCLIC VOLTAMMETRY

From a phenomenological point of view, the study of electrode kinetics involves the determination of the dependence of current on potential and the transition from electronic to ionic conduction. Conduction in the solution is ionic, whereas in the electrodes it is electronic. The transition from one mode of conduction to the other requires a charge transfer across the interface of the electrode. Its rate is controlled by among other things catalytic properties of the surface, the chemisorption or physisorption of species and the concentration and the nature of the reacting species [7]. In a typical experiment the potential is swept and the current is measured. We use cyclic voltammetry as a qualitative tool to test the density or resistance of self-assembled films on the electrode, by investigating the blocking of the oxidation and the reduction processes of a redox pair with respect to the molecular architecture of self-assembled species and the self-assembly time.

MOLECULAR RECOGNITION AT SELF-ASSEMBLED MONOLAYERS

For the purpose of this study, we have defined optimization of an assembly process in the sense that all binding processes occuring at the surface should be specific only and should occur with maximum efficiency: the quantity of the binding partner bound to the surface should be maximized. As a model recognition system, we have

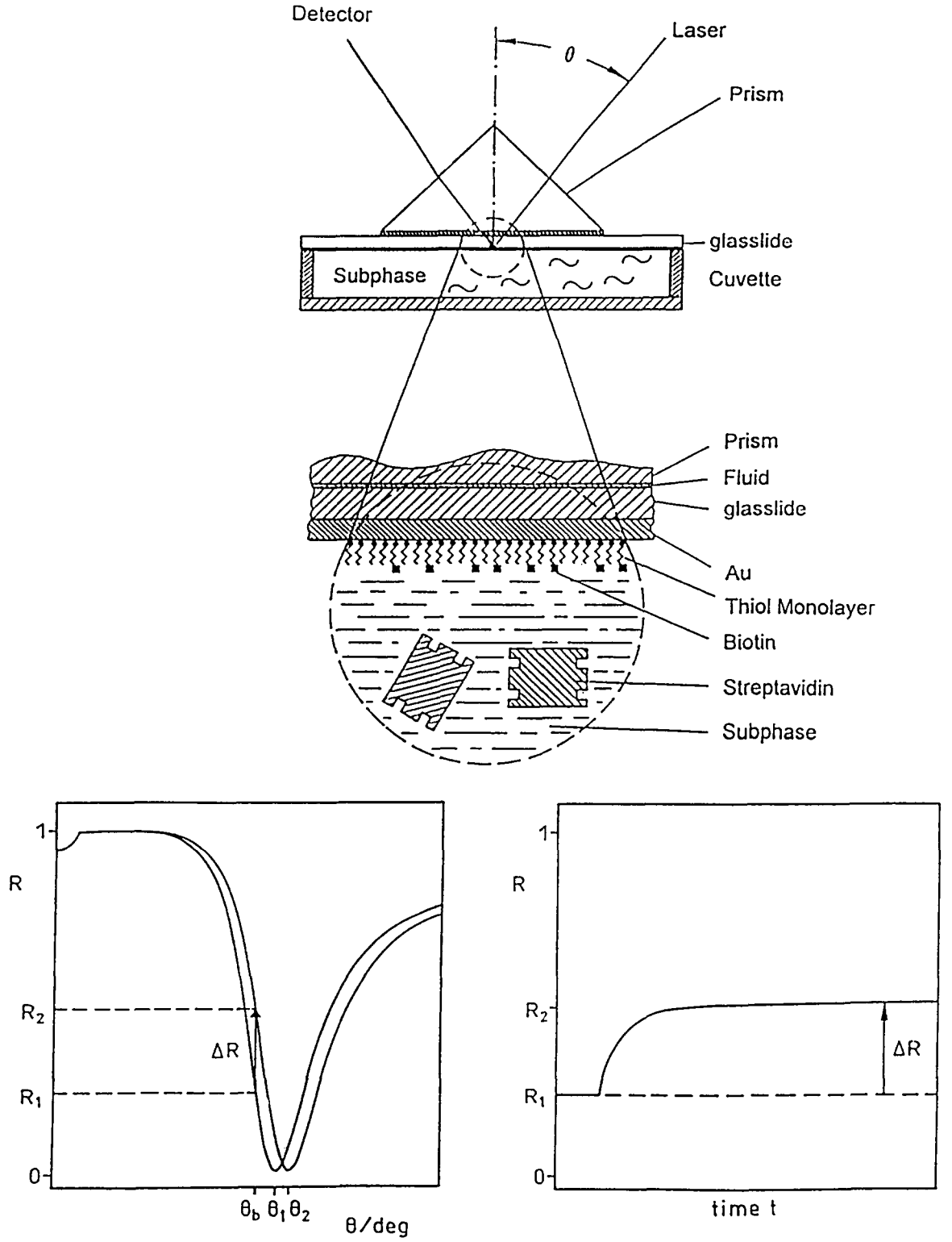

Fig. 3. (top) Schematic of the actual experimental setup used for surface plasmon characterization of multilayer formation. The prism is brought into optical contact with the glass slide, on which the chemical reactions take place, using an index match liquid. (bottom left) Schematic reflectivity curves without and with a dielectric layer on top of the metal, respectively, with different minima positions θ_1 and θ_2. (bottom right) Schematic reflectivity versus time curve obtained with the surface plasmon spectrometer. The addition of a monolayer can be followed in real-time by monitoring the reflected intensity at an angle θ_b.

used the protein streptavidin and its ligand biotin (vitamin H). Streptavidin and its binding to biotin have been very well characterized by a wide variety of methods [27–31]. We have used 10 different sulphur-containing compounds to create a broad range of biotinylated SA monolayers on gold surfaces [10]. These compounds are depicted in Fig. 4. They can be classified into three categories: compounds 1, 2 and 3 are molecules without biotin label but with different binding groups for the gold, namely thiol, sulphide and disulphide. The second class are the compounds 4, 5, 6 and 7 which also carry the different gold-binding functionalities but additionally bear a biotin group bound via a spacer. The third class of molecules, namely compound 8, 9 and 10, consists of disulphides alone with only one of the two possible positions of the molecule labelled with spacer and biotin.

In a first series of experiments the contact angles and the thickness of the SA monolayers (via surface plasmon spectroscopy taking a homogeneous refractive index of n(thiol) = 1·5 and n(protein or peptide) = 1·45 into account) of all compounds have been investigated. The results are shown in Table 1.

It can clearly be seen from Table 1 that the sulphide compounds 3 and 6 do not yield the calculated film thickness even when taking into account a tilt angle of about 30°. Also these compounds show high contact angles which indicate an exposure of the alkyl chains to the surface. These two compounds obviously do not form a closed packed SA monolayer. The monolayers from all other compounds show a hydrophilic surface and the right thicknesses indicating a closely packed SA monolayer. The binding of streptavidin to these SA monolayers has been tested and the resulting thicknesses are listed in Table 1 as well. There is no binding of streptravidin for the compounds 1 and 2 which do not carry a biotin label. This can be attributed to the hydroxy groups present at the surface. Unspecific binding is observed at the sulphide compound 3 exposing partly alkyl chains to the surface. The biotinylated compounds 4–10 exhibit similar behaviour—very little streptavidin binding is observed for compounds 4, 5, 7 and 8, indicating that the choice of thiol or disulphide, and in addition the hydrophilic spacer have very little effect on the binding properties. In contrast, there is very high adsorption of streptavidin to

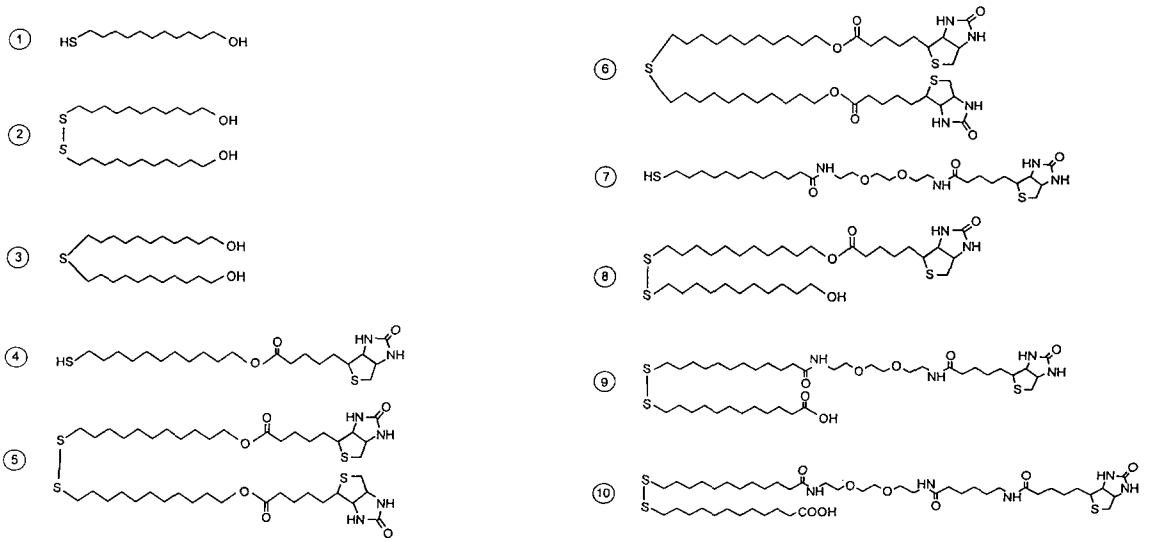

Fig. 4. The structural formulas of the sulphur-based compounds: (1) 11-mercaptoundeconol; (2) bis(11-hydroxyundecyl)disulphide; (3) bis(11-hydroxyundecyl)thioether; (4) biotin-(11-mercapto)undecylester; (5) bis-biotin-(11-mercaptoundecanoylester)disulphide; (6) 11-11'thio-(bis-biotiniundecylester); (7) 12-mercaptododecanoic-(8-biotinoylamino-3,6dioxaoctyl)amide; (8) bis-undecyldisulphido-11-carboxy-11'biotincarboxyester; (9) bis-undecyldisulphido-11-carboyx- 11'(8-iotinamido-3,6-dioxaoctyl)amide; (10) bis(biotinamidocaproyl-amido-3,6-dioxaoctyl)-dodecanamide) disulphide.

TABLE 1 Measured contact angles and measured and calculated monolayer thicknesses of compounds 1–10, as well as the thickness of the subsequently assembled streptavidin layer.

Compound	*d(calc.) (nm)*	*d(exp.) (nm)*	*Contact angle advancing (degree)*	*Contact angle receding (degree)*	*Thickness of adsorbed streptavidin (nm)*
1	1·3	1·1 ± 0·2	16	<5	0 ± 0·2
2	1·3	1·1 ± 0·2	17	<5	0 ± 0·2
3	1·3	0·4 ± 0·2	73	53	1·4 ± 0·2
4	2·3	2·5 ± 0·2	36	10	0·7 ± 0·2
5	2·3	2·4 ± 0·2	29	<10	0·7 ± 0·2
6	2·3	1·3 ± 0·2	65	43	3·3 ± 0·2
7	3·4	3·7 ± 0·3	33	<5	0·9 ± 0·2
8	–	2·3 ± 0·2	29	<5	0·9 ± 0·2
9	–	2·5 ± 0·2	31	<5	2·2 ± 0·2
10	–	3·9 ± 0·3	34	14	2·4 ± 0·2

the sulphide SA monolayer of compound 6. By comparing the asymmetric compounds 8, 9 and 10 one finds an increase in the adsorbed streptavidin thickness with increasing spacer length. This is attributed to a reduction of the steric hindrance for the streptavidin binding to a biotin label sticking out of the monolayer surface. This is also the reason why the binding to compounds 4, 5 and 7 is so small. In order to look closely at the aspect of the steric hindrance two component SA monolayers with changing composition of biotinylated and nonbiotinylated species were investigated. From the thiol, the disulphide and sulphide compounds one or two pairs of materials have been chosen: compounds 1 and 4, 1 and 7 (thiol), compounds 2 and 5 (disulphide) and compounds 3 and 6 (sulphide). The thicknesses of the SA monolayer and the subsequently adsorbed streptavidin films have been measured as a function of the composition of the adsorption solution. It should be pointed out here that it is not necessarily true that the composition within the film corresponds to the one in solution. Figure 5 shows the results for the four different pairs. Comparison of Fig. 5a and b shows that the thiol and disulphide films with identical composition have very similar thicknesses and bind similar quantities of streptavidin. As previously, we see that the sulphide layer (Fig. 5c) exhibits a very different effect: it has a much higher affinity for streptavidin. In all three cases the quantity of streptavidin remains almost constant across the entire composition range. The most interesting case is shown in Fig. 5d, where the characteristics of the SA monolayer prepared by the thiol compounds 1 and 7 is demonstrated. Thiol 7 incorporates a hydrophilic spacer, thus allowing the biotin presented at the surface of the monolayer to stand some distance away from the hydroxyl surface of thiol 1. Diluting these biotin groups results in a large increase in the amount of bound streptavidin at $x = 0.1$. The maximum film thickness of approximately 4 nm corresponds fairly well with the value of 4.5–5 nm obtained for two dimensional crystals of streptavidin [32]. A test whether the binding of streptavidin is specific or nonspecific (by adding streptavidin which had been previously exposed to a solution with free biotin in it to bind into the four binding pockets) has shown that in the case of the sulphide the binding was completely unspecific, whereas the thiols and disulphides show specific binding.

From this results a model (Fig. 6) has been developed which demonstrates the importance of the absence of steric hindrance in binding strepatavidin to the biotin exposed at the surface. The lateral dilution of the biotin and the spacer forcing the biotin to stick out of the surface are essential for optimized binding of the biotin completely into the binding pockets of the streptavidin.

The mixed, optimized system of compounds 7 and 1 has been investigated by building up a multilayer architecture depicted in Fig. 7. The well-known thiol SA monolayer with the bound

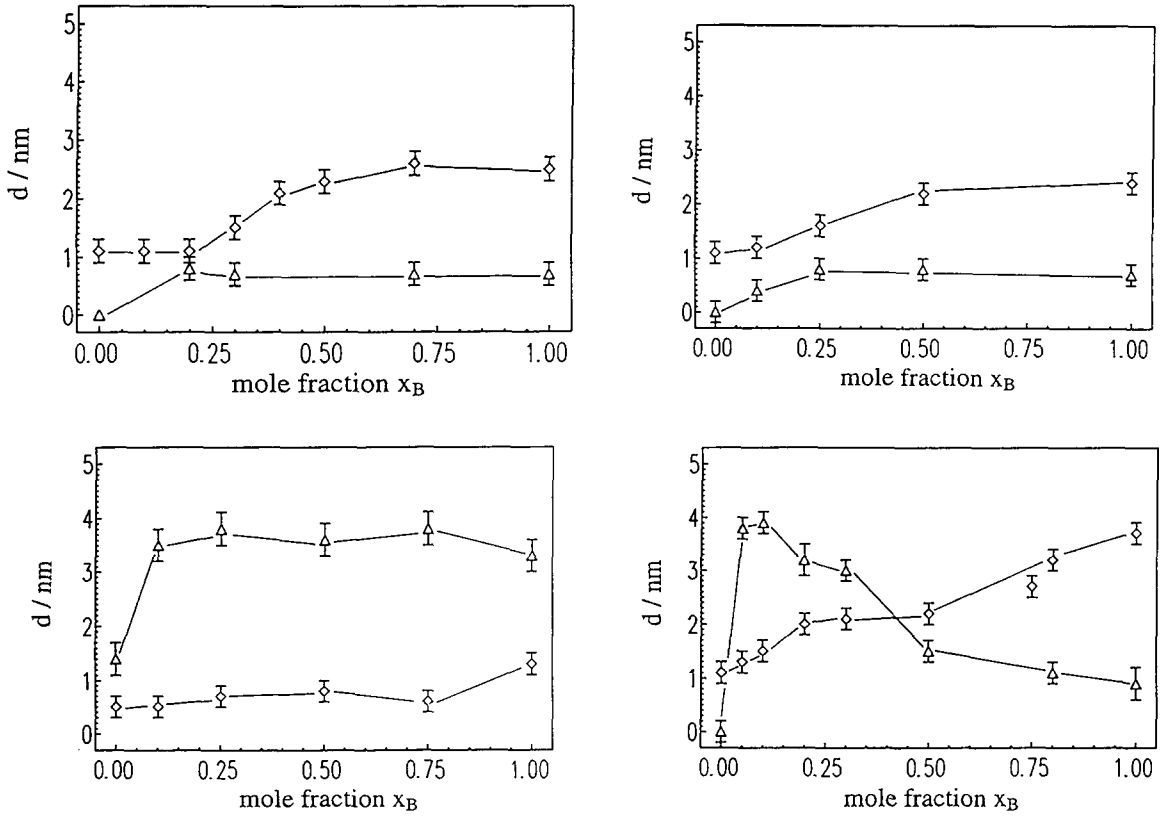

Fig. 5. SA monolayer properties as a function of the composition of the adsorption solution. The thickness d(◇) of the SA monolayers and the subsequently adsorbed streptavidin film (△) of different monolayers are shown as a function of the mole fraction of biotin in the monolayer. Note that the mole fraction x_b of the solution is not necessarily the same mole fraction of biotin in the monolayer (a) thiols 1 and 4, (b) disulphides 2 and 5, (c) sulphides 3 and 6, (d) thiols 1 and 7.

streptavidin is exposed successively to a biotinylated Fab against human chorionic gonadotrophin (Biotin-Fab⟨HCG⟩), the pregnancy hormone human chorionic gonadotrophin (HCG) itself and a mouse monoclonal antibody (Mab⟨HCG⟩) specific for a second epitope of the HCG. The thickness of the individual adsorbed layers are shown as a function of the mole fraction of biotin in the mixed compound 1/7 system in Fig. 8a and b. From Fig. 8a it can be seen that strepatavidin, the biotinylated Fab and the HCG exhibit a similar pattern of binding. There is no binding at the pure mercaptoundecanol film and a maximum binding at a biotin content of x = 0.1, with a gradual reduction in the thickness of the adsorbed film as the biotin content is increased. This behaviour indicates that high densities of binding sites in one layer produces high adsorption of the next layer. In contrast to these layers, the monoclonal antibody exhibits a very different behaviour, with a minimum in adsorbed film thickness at x = 0.1. The specificity of the binding for all species was tested [11] and it was found that all binding reactions had been specific except for the monoclonal antibody, where the extent of unspecific binding was a function of the film composition. The anomalous behaviour of the monoclonal antibody is, therefore, attributed to nonspecific binding.

If in the first layer instead of a biotin label a desthiobiotin label is used the complete layer structure can be separated by rinsing the system with a solution containing free biotin. It takes about a day to regain the desthiobioninylated sample surface [33].

As a final measurement on this system the sensitivity of the multilayer-surface plasmon system for the presence of HCG was tested by investigating the thickness increase of the HCG and the Mab⟨HCG⟩ layer as a function of the

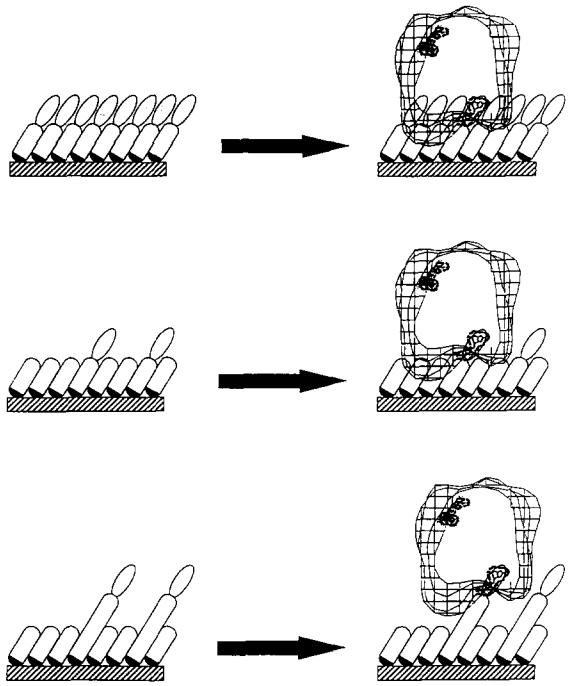

Fig. 6. A schematic representation of the SA monolayers of thiols and the binding of streptavidin to them. The streptavidin data are taken from Ref. 33, with two binding sites shown. The thiol monolayers are drawn approximately to scale. (top) A monolayer of pure thiol 4 is shown here. Binding of streptavidin is severely sterically hindered. (centre) A monolayer of a mixture of thiols 1 and 4 still shows a steric hindrance for binding streptavidin. (bottom) A monolayer of a mixture of thiols 1 and 7. The addition of the spacer allows binding of the streptavidin with no steric hindrance.

concentration of HCG. The adsorption isotherm is depicted in Fig. 9. From this we estimate the detection limit for HCG alone to $2–3 \cdot 10^{-8}$ M and with the additional antibody $1–2 \cdot 10^{-8}$ M, which is still orders of magnitude too small for commercial pregnancy tests, which demands about $5 \cdot 10^{-10}$ M.

SURFACE FUNCTIONALIZATION WITH CYCLODEXTRINS

Cyclodextrins are cyclic oligosaccharides consisting of at least six glucopyranose units which are joined together into a ring. The oligosaccharide ring forms a torus with the primary hydroxyl groups of the glucose residues lying on the narrow end of the torus. The secondary glycopyranose

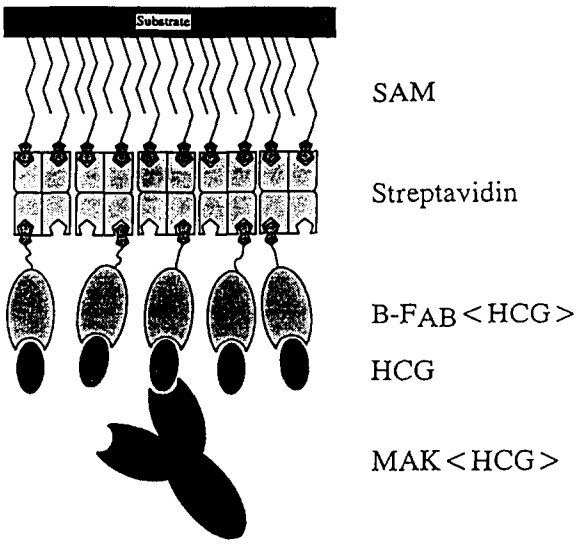

Fig. 7. Schematic representation of the self-assembly multilayer architecture.

hydroxyl groups are located on the wider end. A specific guest complexation can take place in the empty hole of the host torus [34,35]. Figure 10 demonstrates the architecture of the cyclodextrin ring.

We have synthesized and characterized three thiolated β-cyclodextrin derivatives [36] which differ in the length of the spacer between the cyclodextrin ring and the thiol group (mono(6-deoxy-6-thiol) β-cyclodextrin: CD(0), mono(6-deoxy-6-S-thiodecamethylenethiol) β-cyclodextrin: CD(10) and mono(6-deoxy-6-S-thiotriethyleneglycol-thiol) β-cyclodextrin: CD(8)). A fourth compound contained more than one thiolated spacer group, typically between two and four, and is methylated 14 fold at the secondary side (oligo(6-deoxy-6-S-thiodecamethylenethiol)-heptakis(2,3 dimethoxy)β-cyclodextrin: CD_x (10)). Monolayers on gold of all four species have been fabricated by a self-assembly process. Surface plasmon spectroscopy, contact angle measurements and cyclic voltammetry have been performed with these films. Figure 11 demonstrates the results and the interpretation from the surface plasmon spectroscopy (n(cyclodextrin derivatives) = 1.5) and the contact angle investigations in comparison with well-known octadecylmercaptan self-assembled monolayers [1]. The thickness of the monolayer increases with increasing spacer length. A theoretical calculation of the expected film thickness, where we did not

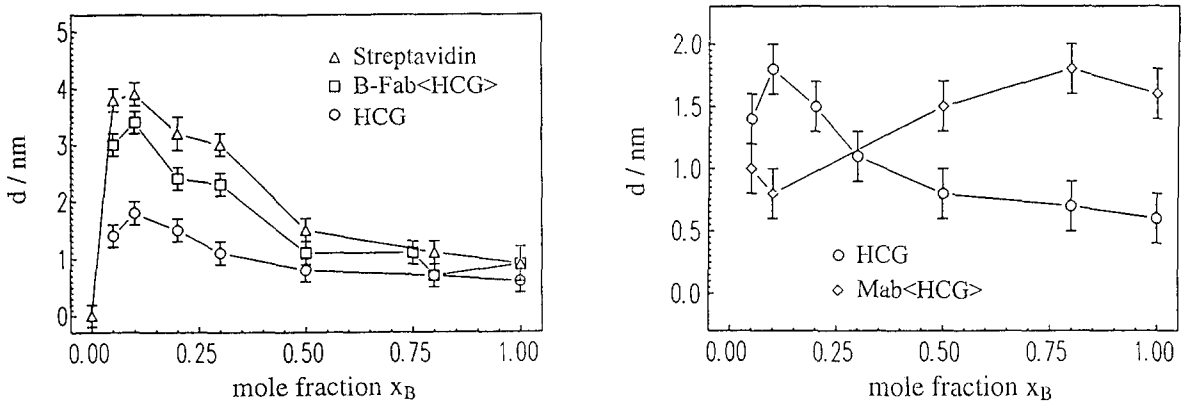

Fig. 8. Multilayer properties as a function of the thiol monolayer composition. The thickness increases of the different monolayers are shown as a function of the mole fraction of biotinylated thiol in the adsorption solution x_b. Lines in the figures are guides to the eyes only. (a) Thickness of the monolayers of the streptavidin (△), the Fab layer (□) and the HCG (○) as a function of the mole fraction x_b. (b) Thickness of the HCG layer (○) and the monoclonal antibody layer (□) as a function of x_b.

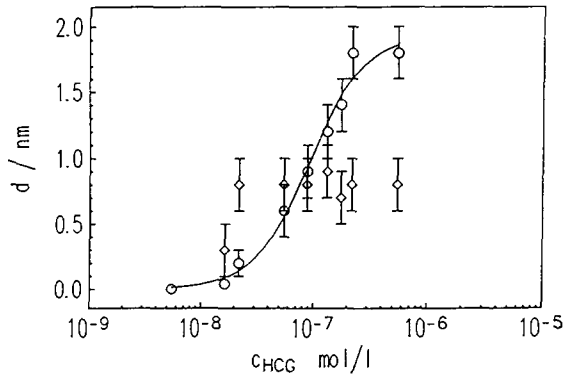

Fig. 9. Adsorption isotherm for HCG (○) and subsequent adsorption of the monoclonal antibody (◇) for multilayers formed with x_b = 0·1.

take into account any tilt angle of the thiols, shows that the spacer chains are stretched and the cyclodextrin rings are tilted at the surface of the sample (Fig. 11). This holds for CD(8) and CD(10). For the CD(0) compound the monolayer thickness indicates an orientation of the cyclodextrin ring more parallel to the surface. In the multichain compound CD_x(10) the cyclodextrins are aligned parallel to the substrate, due to the multibonding. From kinetic measurements, where the completion of the monolayer can be detected by a bend in the adsorption curve (Fig. 13c), we assume that the spacers are preferentially aligned perpendicular to the surface. The typical tilt angles of the alkylthiols on gold are due to interactions between the closely packed alkylchains. These interactions are missing in this

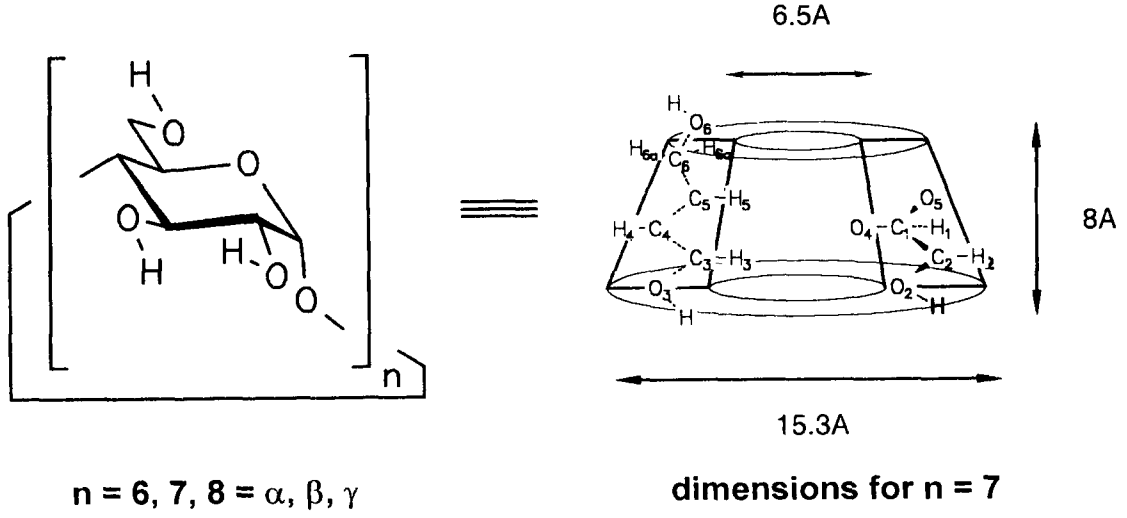

Fig. 10. The chemical structure and the architecture of the cyclodextrin rings: n = 6 is α-, n = 7 is β- and n = 8 is γ-cyclodextrin, respectively.

d [Å] (n=1.5)	θ_A [°] (water)	
20	110	n=18 Au
10	29	Au
29	25	n=10 Au
21	35	n=2 Au
21	50	n=10 Au

Fig. 11. Monolayer thicknesses, advancing contact angle and formation of octadecylmercaptan, CD(0), CD(8), CD(10) and $CD_x(10)$. The monolayer thicknesses and hydrophobicity indicate an elongated alkylchain with tilted cyclodextrins. The cyclodextrins with one thiol group are closely packed, whereas the multichain compound is less densely packed.

case, because only the cyclodextrin-heads are closely packed.

The contact angles show a hydrophilic surface for the cyclodextrin monolayers with one spacer-thiol group, whereas the alkylthiol has a typical hydrophobic surface. The cyclodextrin monolayer assembled from the multichain compound shows a slightly higher contact angle. This is due to the methylation and it may also be possible that this monolayer is somehow less densely packed, and the alkylchains influence the contact angle as well, which can be understood: if two of these multichain species are assembled beside each other, and there is no mobility for the binding thiol group on the gold surface, there is not enough space for a third one to bind in between. This is in agreement with the results from the cyclic voltammetry investigations with a redox system, which is not a guest for the cyclodextrin (Fig. 12). The multichain compound shows the highest oxidation and reduction peaks of the set of scans, which means that here more charges had overcome the barrier of the self-assembled film. Only the bare gold surface shows higher currents. The density of the films made from the one-chain compounds is increasing with increasing spacer length. This is due to the increasing freedom for the cyclodextrins to align at the end of the spacer to form a closely packed film.

The self-assembly kinetics have been studied in two ways, i.e. by plasmon spectroscopy and by cyclic voltammetry. Figure 13 shows the results for compound CD(10). The cyclic voltammograms are depicted in Fig. 13a, where samples with different assembly times have been investigated. The inset in Fig. 13a shows the kinetic curve which was calculated out of the data from Fig. 13a by measuring the integral area between the oxidation and reduction scan and normalizing it to the pure gold surface: 1-(area(thiol)/area(gold)). This curve is very different from the *in situ* measured surface plasmon curve depicted in Fig. 13b, where a double exponential fit of the data is shown. Because of the high concentration of 10^{-4} M the assembly process is not diffusion controlled [10], but controlled by the availability of space for binding, resulting in an exponential behaviour, represented by the first very steep increase. The slower part of the kinetics is due to an alignment of the cyclodextrin heads and to a beginning ad-layer formation. By rinsing a self-assembled film, which had been assembled much longer than necessary for a monolayer formation, the film thickness decreases with rinsing time. The difference between the *in situ* kinetic measurement and the step-by-step measurement with cyclic voltammetry is clear. It indicates the difference between physisorbed molecules, which are washed off after the assembly process in the step-by-step experiment and therefore are not measured, and the chemisorbed molecules, which are not washed off and measured. Whereas in the *in situ* experiment both molecular species are measured together. This behaviour needs further investigation.

First complexation reactions with methylorange and compound CD(0) have been successful: an increase in the optical density of the film was found by incubating the monolayer of cyclodextrins in a dye solution only when the cyclodextrin

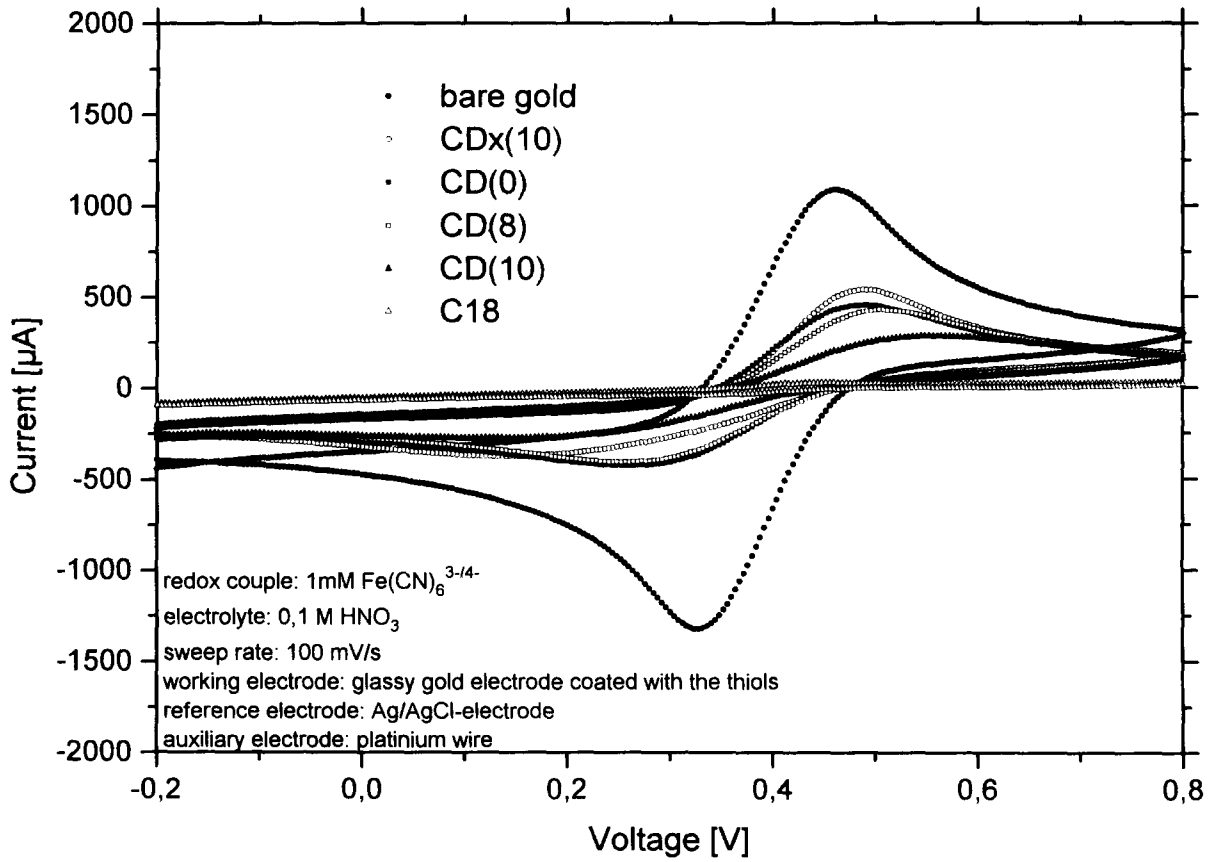

Fig. 12. Cyclic voltammograms for the pure gold surface and all four cyclodextrin derivatives. The experimental details are shown in the inset of the figure.

monolayer was not completely densely packed. Steric hindrance of the cyclodextrin rings in the closely packed condition disables guests to complex into the host rings. In further investigations it has to be tested, whether the dye is located in the cyclodextrin rings or somewhere between or on the rings.

ACKNOWLEDGEMENTS

The authors want to thank Franz-Josef Schmitt and Abraham Ulman for stimulating and helpful discussions. The biotinylated sulphide-, disulphide and thiol compounds for the molecular recognition experiments have been kindly synthesized and provided by H.-J. Guder and L. Angermaier from Boehringer Mannheim GmbH, Werk Tutzingen. Financial support came from Boehringer Mannheim GmbH and the Bundesministerium für Forschung und Technik (Projekt: Nachwachsende Rohstoffe).

REFERENCES

[1] Ulman, A. (1991). *An Introduction to Ultrathin Organic Films.* Academic, New York.

Fig. 13. The self-assembly kinetics for compound CD(10): (a) The cyclic voltammograms for a series of samples which had been given different time for the formation of the SA film and had been carefully rinsed after that. The experimental details are shown in an inset of the figure. The SA kinetic taken from these data are also shown in a second inset. (b) The SA kinetics measured in situ *with the plasmon spectrometer. The line represents a bi-exponential fit to the data.*

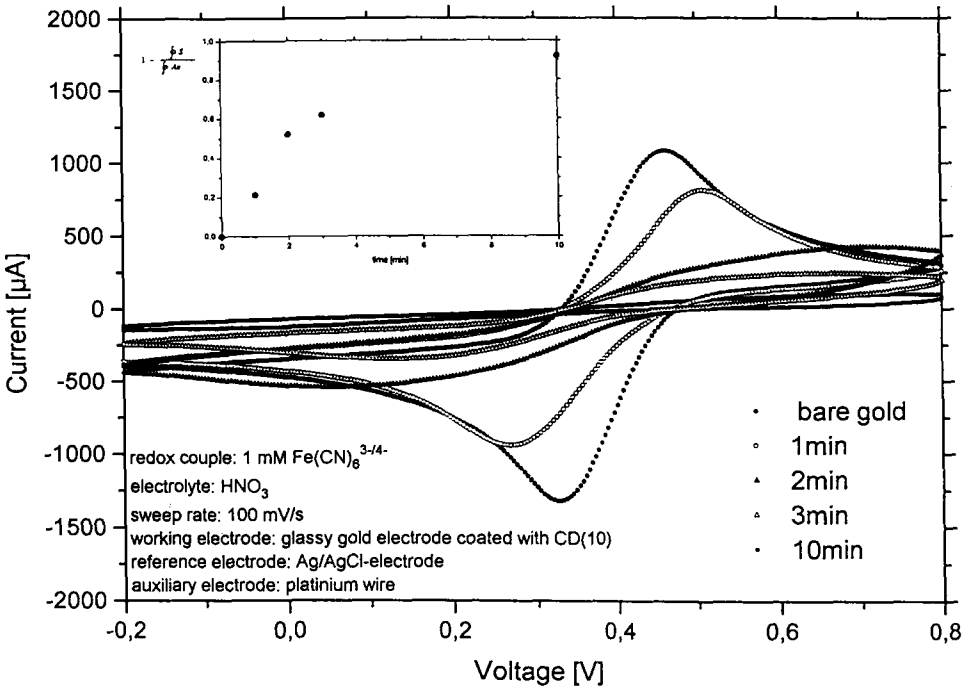
Current [µA]
Voltage [V]
redox couple: 1 mM Fe(CN)6 3-/4-
electrolyte: HNO3
sweep rate: 100 mV/s
working electrode: glassy gold electrode coated with CD(10)
reference electrode: Ag/AgCl-electrode
auxiliary electrode: platinium wire
bare gold
1min
2min
3min
10min

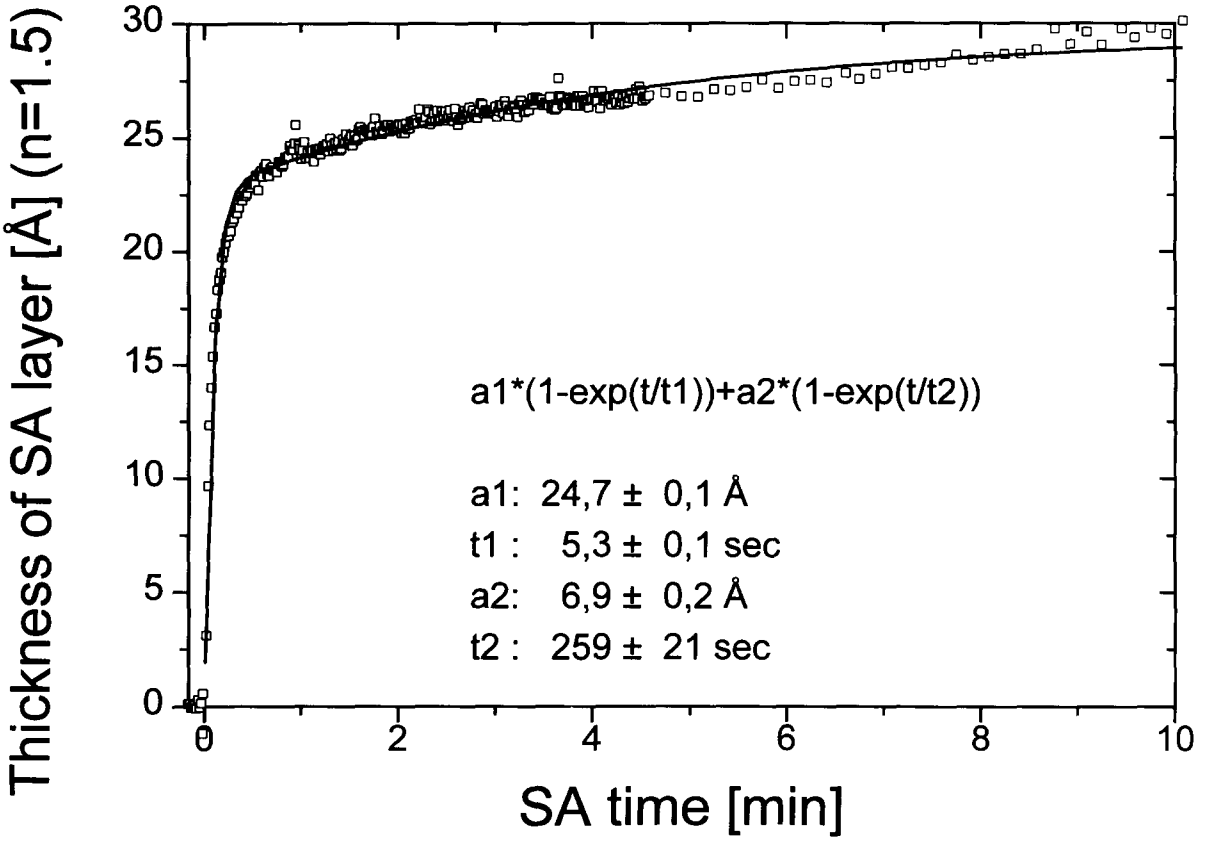
Thickness of SA layer [Å] (n=1.5)
SA time [min]
a1*(1-exp(t/t1))+a2*(1-exp(t/t2))
a1: 24,7 ± 0,1 Å
t1 : 5,3 ± 0,1 sec
a2: 6,9 ± 0,2 Å
t2 : 259 ± 21 sec

[2] Raether, H. (1988). *Surface Plasmons*. Springer, Berlin.
[3] Knoll, W. (1991). *MRS Bulletin,* **XVI 7**, 29.
[4] Rabe, J.P. (1992). *Ultramicroscopy,* **42–44**, 41.
[5] Yang, J., Tamm, L.K., Somlyo, A.P. & Zhao, Z. (1993). *J. Microscopy,* **171**(3), 183.
[6] Harris, T.D., Grober, R.D., Trautman, J.K. & Betzig, E. (1994). *Appl. Spectroscopy,* **48**, 14A.
[7] Greef, R., Peat, R., Peter, L.M., Pletcher, D. & Robinson, J. (1985). *Instrumental Methods in Electrochemistry*. John Wiley & Sons, Chichester.
[8] Neuman, A.W. & Good, R.J. (1979). In: *Surface and Colloid Science* (R.J. Good & R.R. Stromberg, Eds), Plenum, New York.
[9] Whitesides, G.M. & Laibinis, P.E. (1990). *Langmuir,* **6**, 87.
[10] Spinke, J., Liley, M., Schmitt, F.-J., Guder, H.-J., Angermaier, L. & Knoll, W. (1993). *J. Chem. Phys.,* **99**, 7012.
[11] Spinke, J., Liley, M., Guder, H.-J., Angermaier, L. & Knoll, W. (1993). *Langmuir,* **9**, 1821.
[12] Nelles, G., Weisser, M., Back, R., Wenz, G., Mittler-Neher, S. & Knoll, W. 5th European Polymer Federation Symposium on Polymeric Materials, GT2–12.
[13] See any textbook of optics, e.g.: K.D. Möller, University Science Books, Mill Valley.
[14] Burstein, E., Chen, W.P., Chen, Y.J. & Harstein, A. (1974). *J. Vac. Sci. Technol.,* **11**, 1004.
[15] Kretschmann, E. (1972). *Opt. Commun.,* **6**, 185.
[16] Ushioda, S., Sasaki, Y. (1983). *Phys. Rev. B.,* **27**, 1401.
[17] Knobloch, H., Duschl, C. & Knoll, W. (1989). *J. Chem. Phys.,* **91**, 3810.
[18] Hickel, W. & Knoll, W. (1989). *Acta Metall.,* **37**, 2141.
[19] Rothenhäusler, B. & Knoll, W. (1987). *Surf. Sci.,* **191**, 585.
[20] Gordon J.G. II & Swalen, J.D. (1977). *Opt. Commun.,* **22**, 374.
[21] Marcuse, D. (1991). *Theory of Dielectric Optical Waveguides*, 2nd edition. Academic Press Inc., San Diego.
[22] Tien, P.K. (1969). *Rev. Mod. Phys.,* **49**, 361.
[23] Tamir, T. (1979). *Integrated Optics, Topics in Applied Physics*, Vol. 7, 2nd edition. Springer Verlag, Heidelberg.
[24] Hunsperger, R.G. (1984). *Integrated Optics: Theory and Technology*, 2nd edition. Springer Series in Optical Sciences, Springer, Heidelberg.
[25] Boiarski, A.A., Busch, J.R., Bhullar, B.S., Ridgway, R.W., Miller, L.S. & Zulich, A.W. (1993). *Proc. SPIE—Int. Soc. Opt. Eng.,* **1886**, 15.
[26] Fuest, R., Fabricius, N., Hollenbach, U. & Wolf, B. (1993). *Proc. SPIE—Int. Soc. Opt. Eng.,* **1794**, 352.
[27] Hendrickson, W.A., Pähler, A., Smith, J.L., Satow, Y., Merritt, E.A. & Phizackerley, R.P. (1989). *Proc. Natl. Acad. Sci. USA,* **86**, 21990.
[28] Weber, P.C., Ohlendorf, D.H., Wendoloski, J.J. & Salemme, F.R. (1985). *Science,* **243**, 85.
[29] Weber, P.C., Wendoloski, J.J., Pantoliano, M.W. & Salemme, F.R. (1989). *J. Am. Chem. Soc.,* **114**, 3197.
[30] Helm, C.A., Schmitt, F.-J., Israelachvili, J.N. & Knoll, W. (1991). *Makromol. Chem. Symp.,* **46**, 103.
[31] Darst, S.A., Ahlers, M., Meller, P.H., Kubalek, E.W., Blankenburg, R., Ribi, H.O., Ringsdorf, H. & Kornberg, R.D. (1991). *Biophys. J.,* **59**, 387.
[32] Herron, J.N., Müller, W., Paudler, M., Riegler, H., Ringsdorf, H. & Suci, P.A. (1992). *Langmuir,* **8**, 1413.
[33] Spinke, J. (1992). PhD Thesis, Mainz.
[34] Saeger, W. (1980). *Angew. Chem., Int. Ed. Engl.*, **19**, 344.
[35] Wenz, G. (1994). *Chem. Int. Ed. Engl.,* **33**, 803.
[36] Nelles, G., Weisser, M., Back, R., Wohlfart, P., Jaschke, M., Butt, H.-J., Wenz, G. & Mittler-Neher, S., in preparation.